Numerical simulations of potential distribution for elongated insulating dust being charged by drifting plasmas

W. J. Miloch,[1,2] S. V. Vladimirov,[2] H. L. Pécseli,[3] and J. Trulsen[1]
[1]*Institute of Theoretical Astrophysics, University of Oslo, Box 1029 Blindern, N-0315 Oslo, Norway*
[2]*School of Physics, The University of Sydney, Sydney, NSW 2006, Australia*
[3]*Department of Physics, University of Oslo, Box 1048 Blindern, N-0316 Oslo, Norway*
(Received 4 June 2008; published 26 September 2008)

The potential distributions surrounding elongated insulating dust grains being charged by supersonic plasma flows are studied using the particle-in-cell method. The plasma flow introduces an asymmetry in the dust charging. This leads to a complex surface charge distribution on the dust, and to ion focusing in the wake region. We demonstrate that the charge and potential distributions on the dust surface and the wake behind the dust depend on the rod length and dust inclination angle with respect to the flow. The role of the surface charge distribution in the interactions between insulating rods in a plasma is discussed. Our simulations are carried out in two spatial dimensions, treating ions and electrons as individual particles.

DOI: 10.1103/PhysRevE.78.036411 PACS number(s): 52.27.Lw, 52.65.Rr

I. INTRODUCTION

Studies of the potential and plasma density distributions on and around charged dust grains in flowing plasmas are essential for the understanding of interactions in systems comprising many such grains [1,2]. A plasma flow leads to the development of an electric dipole moment on the dust, and to ion focusing in the wake [3–12]. These two features are conspicuous for supersonic flows. It has been shown that, under certain conditions, a potential maximum is formed in the wake region, which can attract downstream dust grains and lead to an alignment of grains in the direction of the flow [4,5,8,10,12].

For simplicity, spherical particles, often modeled as point-like particles, are considered in most theoretical and numerical studies of dusty plasmas [3,5,7,8,13–18]. Such particles prevail also in experimental studies [4,19–21]. However, nonspherical and finite size dust grains are ubiquitous and relevant for space and laboratory plasmas [22,23]. Studies of charging of such grains require a different theoretical approach [24]. An analogous problem can be formulated for larger, complex-shape objects, like satellites or spacecrafts, interacting with space plasma [25–27].

In experiments with rodlike nylon dust grains in rf and dc discharges, it was observed that the dust formed ordered structures [28,29]. In dc discharges all rods were levitated parallel to the electrode, while in rf discharges longer rods were levitated parallel and the shorter ones perpendicular to the electrode. The theoretical models for the charging and interaction of dust rods in flowing plasma, which followed these experiments, addressed conductive grains and neglected the charge distribution on the tips of the rods [30]. Since the rodlike dust in the experiments was made of nylon, a model for highly insulating materials is relevant. A theory describing the charging of an elongated insulator in flowing plasma is hard to develop. In addition, assumptions on the charge distribution in theoretical models of wakes behind rodlike dust have to be made [31]. For these reasons, we use numerical simulations to address this problem in a more consistent way.

In this paper, we present results from particle-in-cell (PIC) numerical simulations of elongated, insulating dust grains in supersonic plasma flows. We simulate the entire charging process of a dust grain in contact with collisionless plasma in two spatial dimensions with no imposed symmetry. By treating electrons and ions as individual particles, we are able to consider the stochastic nature of the whole process within the limitations inherent in the PIC method. We study isolated rods of different lengths and with different inclination angles α with respect to the plasma flow, and we analyze both the charge and potential distributions on the dust surface and in the wake behind the dust. A short discussion is also given on the role of the resulting charge distribution in the interactions between elongated grains. The sizes of simulated grains are comparable with the electron Debye length λ_{De}, and thus the study is directly relevant for larger grains in plasma devices, or meteoroids in space.

For the case of a dust grain placed parallel to the flow our results are qualitatively equivalent to a three dimensional case. For tilted or perpendicular grains, a two dimensional simulation requires careful interpretation since it excludes the dynamics of ions out of the simulated plane, yet our simulations of elongated grains are a good model for grains, or alternatively plates, extended in the direction perpendicular to the simulated plane. This problem will be addressed in more detail in the discussion section.

II. NUMERICAL CODE

The numerical analysis is carried out by a particle-in-cell (PIC) code. The basic features of the code are standard and can be found in the relevant literature [32]. With a more detailed description of the present code given in [11,12], we mention here briefly only some specific features, important for this study.

The problem is analyzed in two spatial dimensions in Cartesian coordinates with Dirichlet boundary condition for the Poisson equation at outer boundaries, where ions and electrons are injected according to *a priori* chosen velocity distributions. Plasma particles are initially distributed internally

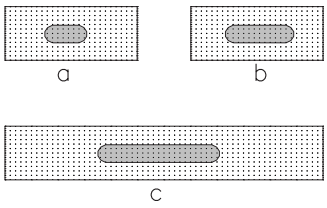

FIG. 1. Sketch of dust shapes considered in the present study. The length of rods is (a) $a \approx 1.5\lambda_{De}$, (b) $a \approx 2.5\lambda_{De}$, and (c) $a \approx 4.5\lambda_{De}$. In all cases the width of rods is $b=0.75\lambda_{De}$.

in the simulation area (except for regions occupied by the dust), in accordance with a Maxwellian velocity distribution. Due to this initialization, we expect initial transients in the system. The simulation area is large compared to the Debye length, and, to mimic an open system, plasma particles can leave freely across any outer boundary. A charged particle hitting the dust surface remains at that position for all later times, contributing to the local charge density. The dust grain is assumed to be rigid and of infinite mass, i.e., it retains its initial shape and remains immobile for the duration of the simulation. We note, however, that the code allows also for a movement of the dust.

We use a 256×256 grid resolution for a simulation area of $50 \times 50\ \lambda_{De}^2$. With a grid spacing of $0.2\lambda_{De}$, we can resolve also the electron Debye length. Our results are presented in normalized units, but when initiating the code we introduce physically relevant parameters, with the exception of the electron to ion mass ratio. The lengths are normalized with the electron Debye length which is fixed in simulations at $\lambda_{De}=10^{-4}$ m. The plasma flow velocity of interest is larger than the ion thermal velocity but much lower than the electron thermal velocity, therefore it suffices to describe it in terms of an ion flow v_d, chosen in the range $v_d \in (0.5, 2.25)C_s$, with C_s denoting the speed of sound. The time resolution is $\Delta t=0.012\omega_{pe}^{-1}$ to prevent electrons from moving more than one grid cell within one time step. We use an ion to electron mass ratio of 120, which is large enough to give credibility to our results [11]. The electron to ion temperature ratio is $\gamma=100$. The plasma density is $n=10^{10}$ m^{-2}, which corresponds to $n=10^{15}$ m^{-3} in a three dimensional system, and the electron temperature is $T_e=0.18$ eV. Thus the plasma in our simulations is typical for dc glow or rf discharge plasmas.

We analyze elongated dust grains of three different lengths $a \approx 1.5$, 2.5, and 4.5 λ_{De} that will be referred to as the short, medium, and long rods, respectively, see also Figs. 1(a)–1(c). The width of a rod is $b=0.75\lambda_{De}$ for all the grains. The dust grain is placed inside the simulation area with different inclination angles with respect to the ion flow, $\alpha \in (0, 90)°$. A summary of parameters of the simulated plasma is given in Table I.

The code is run until steady state conditions are reached, typically after three ion plasma periods τ_i for subsonic flows. Since the ion flow acts as an energy input to the system, we are particularly interested in the asymptotic charging characteristics of dust grains for fast ion flows. For fast flows we find asymptotic conditions for the total dust charge after approximately nine ion plasma periods for spherical grains, and even later for elongated grains. In order to have statistically satisfactory results, we run our code typically for 50 ion plasma periods.

TABLE I. Summary of the simulated plasma parameters.

Simulation area dimension	$L_x=L_y=5\times10^{-3}$ m
Electron Debye length	$\lambda_{De}=10^{-4}$ m
Electron temperature	$T_e=0.18$ eV
Temperature ratio	$T_e/T_i=100$
Ion to electron mass ratio	$m_i/m_e=120$
Electron plasma frequency	$\omega_{pe}=1.79\times10^9$ s^{-1}
Ion plasma frequency	$\omega_{pe}=1.63\times10^8$ s^{-1}
Plasma density	$n=10^{10}$ m^{-2}
Dust lengths	$a \approx 1.5$, 2.5, and 4.5 λ_{De}
Dust width	$b=0.75\lambda_{De}$

III. NUMERICAL RESULTS

For the short rod with zero inclination angle with respect to the moderate ion flows ($v_d \leqslant 1.5C_s$), we observe the development of positive surface charge regions on the dust sides tangential to the flow. These regions have periodically distributed positive potential maxima as shown in Fig. 2. The potential in Fig. 2, and in other figures, is normalized by the floating potential of a large probe in a stationary plasma,

$$\Phi_{fl} = -\frac{\kappa T_e}{e}\left[\ln\left(\frac{M}{2\pi m}\right)+1\right]. \tag{1}$$

This result takes into account also the ion acceleration in the pre-sheath and assumes the cold ions reaching the probe at the Bohm speed [33]. Hence the floating potential does not depend on the electron to ion temperature ratio. Since $\Phi_{fl}<0$, the positive potential maxima appear with negative values in Fig. 2. With increasing ion drift velocity, these positive regions shift towards the rear of the rod, eventually

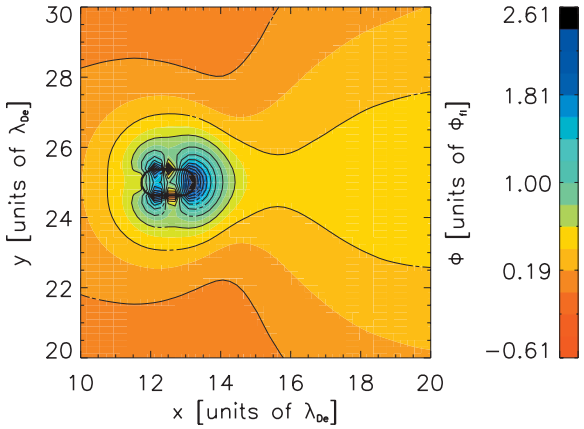

FIG. 2. (Color) Potential variation for a plasma with ion drift velocity $v_d=1.0C_s$ around an insulating dust with the shape given by Fig. 1(a) with zero inclination angle $\alpha=0°$. Potential is normalized with the floating potential $\Phi_{fl}<0$ consistent with our previous results [11]. The ion drift is in the positive x direction.

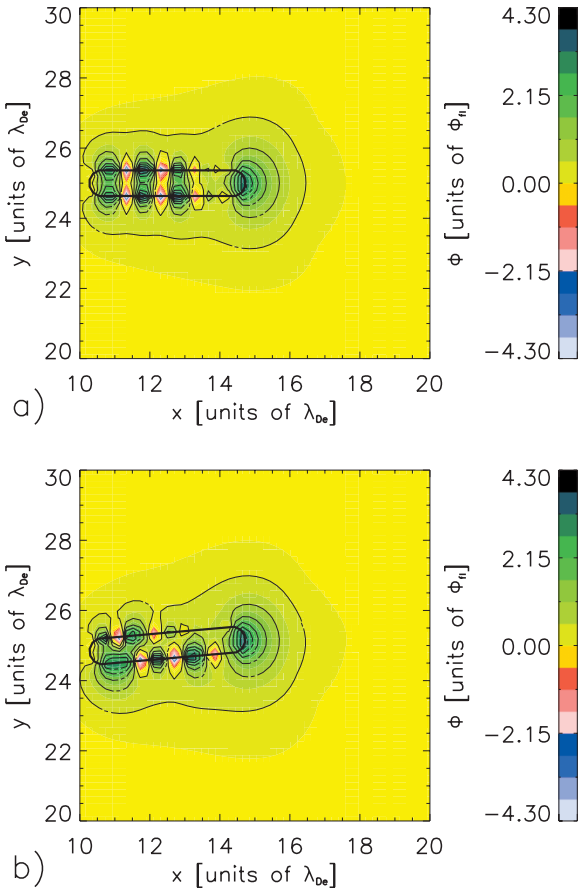

FIG. 3. (Color) Potential variation for a plasma with ion drift velocity $v_d=2.0C_s$ around an insulating dust with the shape given by Fig. 1(c) for inclination angles $\alpha=0°$ (a) and $\alpha=5°$ (b). Potential is normalized as in Fig. 2. The ion drift is in the positive x direction.

to disappear and the resulting potential distribution to resemble the case of an isolated spherical grain [11].

Positive surface charge regions are found also for medium and long rods that are parallel to the ion flow, but they do not disappear with increased ion drift velocity, at least within the simulated velocity range. On these rods, additional maxima in the potential develop further downstream on the dust surface, see Fig. 3(a), and they are observed already for subsonic flows. With the development of the new maxima, the foremost maxima are enhanced and move towards the front of the rod, i.e., against the ion flow. The positions of the maxima are similar on the medium and long rods, but on the short rod they are located consistently closer to the front of the rod. The position and period of the maxima are linear functions of the ion drift velocity. The distance between two successive maxima increases with the ion drift velocity. The distance between the front of the rod and the foremost maxima increases at a similar rate.

The symmetry in the surface charge distribution is broken already for small inclination angles α. On the shadow side of the rod, the positive maxima in the potential distribution are shifted towards the rear of the rod, while on the side facing the flow they become less pronounced and move towards the front of the rod; see Fig. 3(b). With increasing α, the side facing the flow acquires more positive charge, which is distributed more homogeneously. When the inclination angle exceeds a critical value the maxima on the shadow side disappear. The critical inclination angle α_c varies with the ion drift velocity, being smaller for higher Mach numbers, but we do not find the Mach cone angle and α_c to be related.

The ion flow leads to a polarization of the charge on the dust surface. For the case of the long rod with zero inclination angle, the charges on the front q_f and the rear end q_r, as well as the total charge on the rod q_t, were calculated for different ion drift velocities. The front and rear charges correspond to regions that are non-tangential to the ion drift velocity on the grain from Fig. 1(c). Each charge was averaged over a time interval $t \in (42,49)\tau_i$. The corresponding electric dipole moment $\vec{p}$ on the rod was also calculated using the formula

$$\vec{p} = \sum_{i=1}^{n} \tilde{q}_i \vec{r}_i, \tag{2}$$

where the summation is over all charged particles collected on the dust surface, and $\tilde{q}$ is the difference between the actual charge on the dust surface and the mean local charge: $\tilde{q}=q-q_t/n$, i.e., $\Sigma_{i=1}^{n}\tilde{q}_i=0$. The results are given in Table II, with the charge presented in units of the two dimensional elementary charge q_0, given by

$$q_0 = e[n_{0(3D)}]^{1/3}, \tag{3}$$

where e and $n_{0(3D)}$ are the elementary charge and plasma density in the three dimensional system, respectively. The physical dimension of q_0 is $[q_0]=\mathrm{C/m}$. For the electric dipole moment, we present its magnitude $|\vec{p}|$, normalized with $q_0\lambda_{\mathrm{De}}$, and note that $\vec{p}$ is directed against the flow. It can be inferred from Table II that the absolute values of the charge on the front and rear ends of the rod, and the total charge on the rod increase with the ion flow, and that the electric dipole moment has a maximum at $v_d=2.0C_s$. This shows that the charge accumulated at the sides of the dust influences the dipole moment in the surface charge distribution.

The electric dipole moment and total charge on the long rod were measured for different inclination angles α, for the ion drift velocities $v_d=1.25C_s$ and $v_d=2.0C_s$. The results shown in Table III are averaged over a time interval $t \in (42,49)\tau_i$. In both cases, the total charge q_t and the electric dipole moment increase with the inclination angle α for $\alpha \in (25,45)°$, but the trend is not clear for $\alpha<25°$. The angle β between $\vec{p}$ and the direction antiparallel to the ion flow is maximum for $\alpha \in (25°,30°)$. It is close to zero at $\alpha=0°$ and $\alpha=90°$, with nonzero values of β being attributed to the stochastic nature of dust charging. For rods placed perpendicular to the flow, the charge polarization is maximal.

Symmetric wakes in the ion density are observed for $\alpha=0°$ and $\alpha=90°$, but they are topologically different in the two cases. For a rod parallel to the flow, a part of the ion population is lost on both sides of the dust, contributing to the positive surface charge density regions; see Figs. 3(a) and 4. Only ions reaching the rear end of the dust can be focused behind the dust. The ions streaming out from the focal region give rise to a new symmetric perturbation in the ion density

TABLE II. The charge and electric dipole moment on the long rod with zero inclination angle ($\alpha=0°$) for different ion drift velocities v_d. q_f and q_r are the charge on the front and rear end of the rod, respectively. q_t is the total charge on the rod, and $|\vec{p}|$ is the normalized magnitude of the electric dipole moment. The data were averaged over a time interval $t \in (42,49)\tau_i$. The charge is presented in units of a two dimensional elementary charge.

v_d [units of C_s]	q_f [units of q_0]	q_r [units of q_0]	q_t [units of q_0]	$\lvert\vec{p}\rvert$ [units of $q_0\lambda_{De}$]
0.50	827	−459	−1425	176
0.75	1371	−1036	−1522	365
1.00	1739	−1937	−1732	907
1.25	1882	−2375	−1970	1035
1.50	2242	−2877	−2136	1218
1.75	2319	−3089	−2189	1239
2.00	2399	−3265	−2306	1321
2.25	2595	−3537	−2303	1109

located downstream. In the case of the rod oriented perpendicular to the ion flow, we find that the reduction in the ion density in the shadow of the rod is substantial, resulting in the back side of the dust being charged negatively. The ion focusing is stronger in this case, with a spatially larger focusing region located further downstream than in the previous case.

Tilting of the rod introduces an asymmetry in the wake behind the dust grain. Figure 5 shows that a part of the ion population in the vicinity of the dust is lost to the positive surface charge density regions on the shadow side of the rod. The ion focusing region is distorted, and this gives rise to asymmetric perturbations in the density and potential distributions; see Figs. 5 and 6. In particular, an asymmetry is clearly visible for ions streaming out from the ion focusing region. We find by inspection of Fig. 6(c) that a fraction of the ions emerge as a partially collimated "jet," see the region around $(x,y)=(17,28)\lambda_{De}$. We note these ions by a slightly enhanced local ion density. The ion beam is particularly conspicuous in the vector plots showing the locally averaged ion velocity vector. We interpret this part of the ion population as a fraction of the incoming ions being focused (similar to the case of electrostatic lenses) by the asymmetric electrostatic field around the elongated tilted dust grains [34].

IV. DISCUSSION AND CONCLUSIONS

The potential and plasma density variations on and around insulating elongated dust grains in drifting plasmas were studied with PIC simulations. The charge and potential distributions on the dust surface and the wake formation were investigated for rods of different lengths and different inclination angles α with respect to the ion flow. In the presence of an ion drift, positive charge accumulates on the rod side that is facing the flow, while other sides are initially negatively charged. The trajectories of ions are distorted in the

TABLE III. The total charge q_t and the magnitude of the electric dipole moment $|\vec{p}|$ on the long rod for different angles of inclination α. The data for two ion drift velocities $v_d=1.25C_s$ and $v_d=2.0C_s$ are shown. In all cases $\vec{p}$ is oriented against the flow with β being the angle between $\vec{p}$ and the direction antiparallel to the flow. The data were averaged over $t \in (42,49)\tau_i$.

	$v_d=1.25C_s$			$v_d=2.00C_s$		
α [deg]	q_t [units of q_0]	$\lvert\vec{p}\rvert$ [units of $q_0\lambda_{De}$]	β [deg]	q_t [units of q_0]	$\lvert\vec{p}\rvert$ [units of $q_0\lambda_{De}$]	β [deg]
0	−1970	1035	2	−2306	1321	1
5	−2025	1053	10	−2353	1582	13
10	−2040	1106	15	−2350	1629	16
15	−2189	1137	28	−2781	2723	19
20	−2150	1048	26	−2519	1952	26
25	−2162	1173	38	−2491	1985	31
30	−2188	1224	33	−2599	2392	32
35	−2289	1402	27	−2624	2795	30
40	−2302	1546	27	−2805	3601	22
45	−2411	1606	26	−2900	3717	19
90	−2413	2665	−1	−2566	3655	0

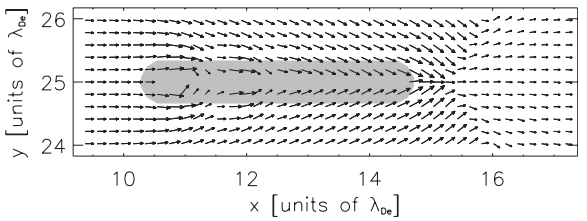

FIG. 4. Averaged ion velocity around the long dust with zero inclination angle $\alpha=0°$. The ion drift velocity is $v_d=1.75C_s$. The ion velocities are averaged over a time interval $t=0.7\tau_i$ at the end of simulation, and over grid cells by weighting the ion velocities to the nearest grid points. Since the dust surface is not placed directly on grid points, the average velocity for ions close to the surface appear to be plotted within the dust. The dust area is marked gray.

vicinity of the dust by strong local electric fields. The ions are deflected away from the front end of the rod and attracted by negatively charged regions further downstream. In the case of spherical grains these ions would contribute to an ion focusing region behind the dust, but for rodlike grains the ions can be focused on the rod surface. As a result, positively charged regions and corresponding maxima in the potential distributions develop on the sides of the rod. These maxima deflect the incoming ions and other regions of positive charge can be created further downstream on longer rods. The vector plots of the average ion velocity confirm this interpretation. From Fig. 4 the motion of ions can be inferred, as well as an ion focusing region behind the dust. For a plasma with cold ions as studied here ($T_e/T_i=100$), the potential maxima are pronounced. They exist also for lower temperature ratios, although they are less pronounced there due to the ion thermal spread in velocities.

The distance between successive potential maxima is proportional to the ion drift velocity, which confirms that they are created mainly due to the bending of ion trajectories. The positions of maxima on the short rod are altered by the strong electric fields due to the negatively charged rear of the

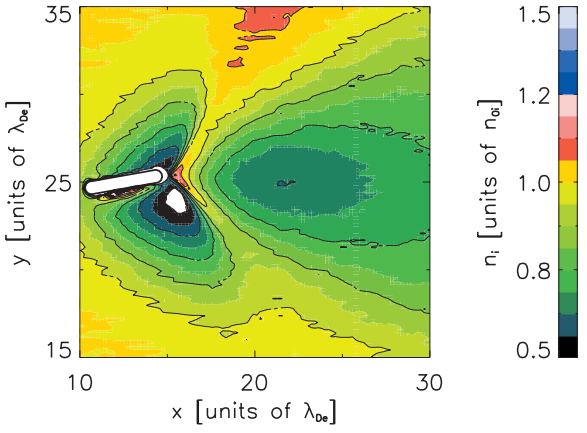

FIG. 5. (Color) Averaged ion density for a plasma with ion drift velocity $v_d=2.0C_s$ around the long rod with the inclination angle $\alpha=10°$. The white regions in the density plot represent density ratios $n_i/n_{i0}<0.5$. The ion drift is in the positive x direction. For a better visualization, the color scale is inverted here as compared to the figures of potentials.

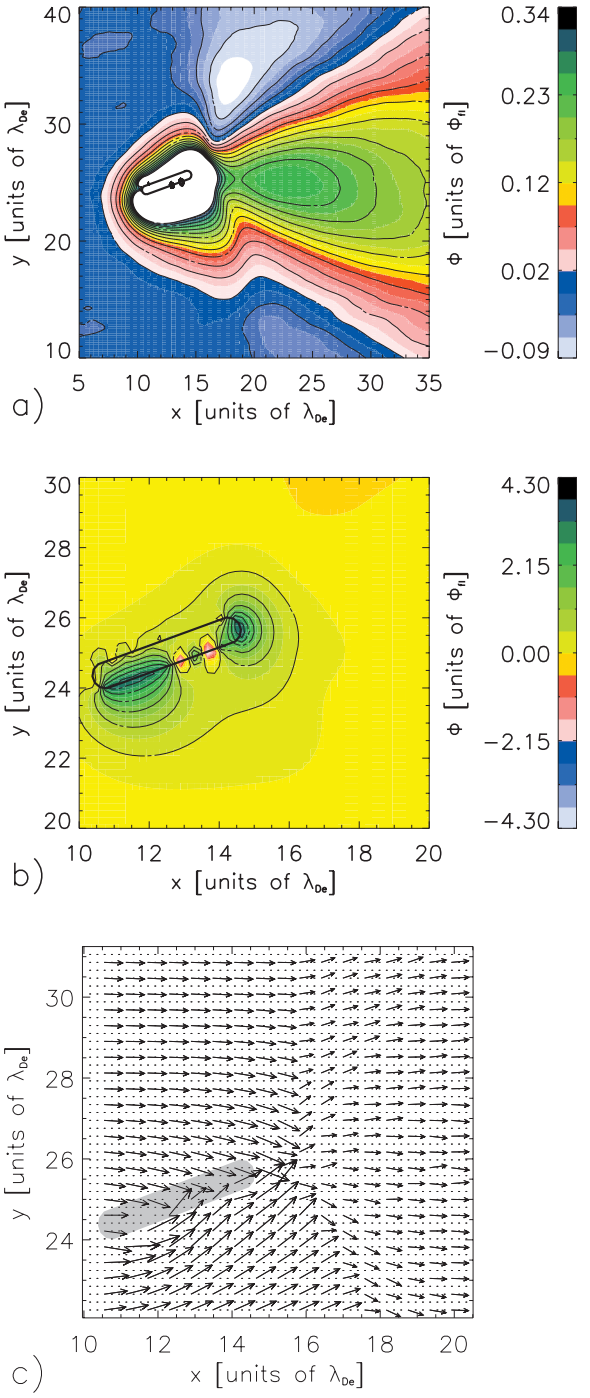

FIG. 6. (Color) Potential variation (a), (b) and averaged ion velocities (c) for a plasma with ion drift velocity $v_d=2.0C_s$ around an insulating dust with the shape given by Fig. 1(c) and the inclination angle $\alpha=20°$. Potential is normalized as in Fig. 2. In (a), only potentials close to the plasma potential $\Phi=0$ are colored. The ion drift is in the positive x direction. The figure (b) shows the region close to the dust with the same color scale as in Fig. 3. The ion velocities in (c) are averaged over a time interval $t=0.7\tau_i$ at the end of simulation, and over grid cells by weighting the ion velocities to the nearest grid points. For a better representation the velocities are shown for a reduced number of grid points. Since the dust surface is not placed directly on grid points, the average velocity for ions that are close to the surface appear to be plotted within the dust. The dust area is marked grey.

grain, and thus they are closer to the front of the rod than for longer rods. With increasing ion drift velocity, the maxima are shifted further downstream, and disappear eventually on the small grain. In the latter case all the ions are focused in the wake behind the dust.

The charge is periodically distributed on the rod with zero inclination angle, with the charge being polarized on the rod ends. The charge polarization is stronger with increasing ion flow velocity, but the electric dipole moment has a maximum at $v_d \approx 2C_s$. This result is attributed to the charge distribution on the dust surface, which partially cancels the electric dipole moment. Therefore even though the absolute charge values on both ends of the rod, q_f and q_r, increase with the ion flow velocity, the charge accumulated on sides of the dust governs the dipole moment of the surface charge distribution. The representation of the insulating rod by the charge assigned only to its both ends is insufficient. On the other hand, in some simplified analytical investigations, a rodlike dipole can be considered as a dumpbell-shaped particle, with the charges q_f and q_r at the ends. Our simulations provide information on the limits of such an approximation.

The symmetry in the surface charge distribution is destroyed on tilted rods. On the shadow side, the ion trajectories are bent as for rods with zero inclination angles, but this time the ions hit the dust surface further away from the front end. At the same time, the maxima on the side facing the flow are located closer to the front of the rod. These maxima diminish with increasing α since the ion flow charges this surface more homogeneously. The polarization of the charge on the dust is largest for high inclination angles, when the shadow side is charged highly negatively, and the ions are focused in the wake. The magnitude and direction of the electric dipole moment change with the inclination angle α. The angle β between the electric dipole moment and direction antiparallel to the ion flow has the maximum for $\alpha \in (25, 30°)$. For larger angles the ion trajectories are not distorted sufficiently to contribute to the complex charge distribution on the shadow side of the dust, and the rod becomes more polarized, as reflected in the decrease in β. For a rod perpendicular to the flow, an electric dipole moment antiparallel to the flow direction is recovered. The ions are subjected to strong electric fields on the shadow side of the dust, and thus we do not find a correlation between the critical angle of inclination α_c (where the maxima on the shadow side disappear) and the Mach cone angle $\gamma = \sin^{-1}(C_s/v_d)$.

Although the basic features of the wake further downstream from the dust grain are similar to those for spherical dust grains [11], there are notable differences close to the dust surface, where the regions of enhanced ion density are localized. The asymmetry of the wake is substantial for tilted rods. The ion focusing region is distorted and the ions streaming out of the focal region create an asymmetric wake in the electrostatic potential. In particular, ion jets with highly uniform velocities can have important implications for long range interactions of elongated dust grains.

The wake asymmetry behind tilted rods was also argued by a theoretical approach using a linear response function, where an oscillating wake pattern was reported [31,35]. We do not observe these oscillations in the present analysis. Our results are different due to the nonlinearity, finite size of the grain, and self-consistent charging of the rods. The charging of a finite sized rod in flowing plasmas leads to highly charged regions on the dust surface, and the ion trajectories are subjected to strong electric fields in the vicinity of the dust. There is also a substantial depletion in the ion and electron densities in the shadow of the flow. Thus, the basic assumptions of the linear response theory are violated.

The charge distribution depends on the ion drift velocity, angle of inclination α, and length of the rod. The complex charge distribution has important consequences for the interactions between rodlike particles in flowing plasmas. It was shown before that rodlike dust particles may exhibit rotational motion when organized in chains [36,37]. In those studies rods were assumed to have constant charges on their tips. Changes in the surface charge distribution may alter such oscillations, by letting the interactions between rods be a function of the inclination angles of two neighboring rods. In other theoretical studies of interactions between two conducting rods, it was concluded that the main contribution is due to the total charge on the rod [30]. This does not have to be the case for insulating rods polarized due to the ion flow. We have shown that the charge on insulating dust grains is an important variable, which may lead to nontrivial interactions between rods, when included self-consistently in the analysis. However, more studies are necessary to address this problem. We note that our code is capable for studies of interactions between two rodlike particles, and such studies are planned for the near future.

The positions of the potential maxima on the dust surface are a function of α. A slightly tilted rod will have a broken symmetry in the charge distribution. Thus the charge distribution on rods with $\alpha \approx 0°$ is very sensitive to changes in α. However, for large α the changes in the charge distributions are much less pronounced, and one can argue that for $\alpha \approx 90°$ the distribution will be insensitive to small α variations. Dust rods with $\alpha = 90°$ would correspond to rods placed parallel to the electrode in dc discharges. In such experiments, a parallel orientation of the rods was actually found to be a favorable configuration. A charged object moving with respect to the plasma is decelerated in part by the electric field it creates by polarizing the surrounding medium [18], and also by the net momentum impact of plasma particles hitting the surface of the object. For velocities considered in the present work, the electron impact is close to isotropic and the dominant momentum flux is due to the anisotropic ion impacts. This process has been studied by numerical methods as described in the literature [38], although most of these results refer to spherical objects. The electric field and drag force present in the experiments also have a significant role and can for instance make the rod rotate.

The flowing plasma exerts an ion drag force on the elongated dust. This force will be particularly strong for tilted grains. The asymmetric charge deposition on the sides of the dust will lead to the rotation of the dust and align it perpendicular to the flow. For tilted grains, this is valid for both components of the ion drag force: the collection force, due to an asymmetric ion deposition, and the Coulomb force, for which negatively charged parts of the rod will be attracted by the bent ion trajectories. However, the dust was assumed to

be immobile in our simulations, and the ion drag force acting on the dust was not measured.

Our results are two-dimensional, and this should be remembered when interpreting the results. As mentioned earlier, the results for rods parallel to the flow are qualitatively equivalent to a three dimensional case. When the rod is tilted, the results will be applicable for dust grains or objects that are extended in the direction perpendicular to the simulated plane. Otherwise, one needs to consider also the ion flow above and below the rod. Such flows would correspond to flows around spherical grains that were simulated before [11]. Therefore we can expect that for larger ion flow velocities there will be a wake region just behind the dust, followed by the ion focusing region. For the case of a rod, there will be a focusing line parallel to the rod surface in addition to the wake demonstrated in the present study. If these two wakes can be superimposed, then in the vicinity of the grain the wake will be similar to that in our analysis.

ACKNOWLEDGMENTS

This work was partially supported by the Norwegian Research Council, NFR, and by the Australian Research Council, ARC.

[1] P. K. Shukla and A. A. Mamun, *Introduction to Dusty Plasmas* (Institute of Physics Publishing, Bristol, 2002).
[2] S. V. Vladimirov, K. Ostrikov, and A. A. Samarian, *Physics and Applications of Complex Plasmas* (Imperial College Press, London, 2005).
[3] S. V. Vladimirov and M. Nambu, Phys. Rev. E **52**, R2172 (1995).
[4] A. Melzer, V. A. Schweigert, I. V. Schweigert, A. Homann, S. Peters, and A. Piel, Phys. Rev. E **54**, R46 (1996).
[5] O. Ishihara and S. V. Vladimirov, Phys. Plasmas **4**, 69 (1997).
[6] A. V. Ivlev, G. Morfill, and V. E. Fortov, Phys. Plasmas **6**, 1415 (1999).
[7] G. Lapenta, Phys. Plasmas **6**, 1442 (1999).
[8] S. A. Maiorov, S. V. Vladimirov, and N. F. Cramer, Phys. Rev. E **63**, 017401 (2000).
[9] J. W. Manweiler, T. P. Armstrong, and T. E. Cravens, J. Plasma Phys. **63**, 269 (2000).
[10] G. A. Hebner and M. E. Riley, Phys. Rev. E **69**, 026405 (2004).
[11] W. J. Miloch, H. L. Pécseli, and J. Trulsen, Nonlinear Processes Geophys. **14**, 575 (2007).
[12] W. J. Miloch, J. Trulsen, and H. L. Pécseli, Phys. Rev. E **77**, 056408 (2008).
[13] M. Lampe, G. Joyce, G. Ganguli, and V. Gavrishchaka, Phys. Plasmas **7**, 3851 (2000).
[14] D. Winske, W. Daughton, D. S. Lemons, and M. S. Murillo, Phys. Plasmas **7**, 2320 (2000).
[15] O. Ishihara, S. V. Vladimirov, and N. F. Cramer, Phys. Rev. E **61**, 7246 (2000).
[16] I. V. Schweigert, V. A. Schweigert, and F. M. Peeters, Phys. Plasmas **12**, 113501 (2005).
[17] W. J. Miloch, S. V. Vladimirov, H. L. Pécseli, and J. Trulsen, Phys. Rev. E **77**, 065401(R) (2008).
[18] P. Guio, W. J. Miloch, H. L. Pécseli, and J. Trulsen, Phys. Rev. E **78**, 016401 (2008).
[19] G. A. Hebner, M. E. Riley, and B. M. Marder, Phys. Rev. E **68**, 016403 (2003).
[20] A. A. Samarian and S. V. Vladimirov, Phys. Rev. E **67**, 066404 (2003).
[21] A. Piel and A. Melzer, Plasma Phys. Controlled Fusion **44**, R1 (2002).
[22] C. R. Stark, H. E. Potts, and D. A. Diver, Astron. Astrophys. **457**, 365 (2006).
[23] M. Horányi, Annu. Rev. Astron. Astrophys. **34**, 383 (1996).
[24] H. Zahed, J. Mahmoodi, and S. Sobhanian, Phys. Plasmas **13**, 053505 (2006).
[25] K. R. Svenes and J. Trøim, Planet. Space Sci. **42**, 81 (1994).
[26] F. Melandsø and J. Goree, Phys. Rev. E **52**, 5312 (1995).
[27] J. J. Berthelier and J. F. Roussel, J. Geophys. Res. **109**, A01105 (2004).
[28] V. I. Molotkov, A. P. Nefedov, M. Y. Pustyl'nik, V. M. Torchinsky, V. E. Fortov, A. G. Khrapak, and K. Yoshino, Pis'ma Zh. Eksp. Teor. Fiz. **71**, 152 (2000); JETP Lett. **71**, 102 (2000).
[29] B. M. Annaratone *et al.*, Phys. Rev. E **63**, 036406 (2001).
[30] A. V. Ivlev, A. G. Khrapak, S. A. Khrapak, B. M. Annaratone, G. Morfill, and K. Yoshino, Phys. Rev. E **68**, 026403 (2003).
[31] S. V. Vladimirov and M. Nambu, Phys. Rev. E **64**, 026403 (2001).
[32] C. K. Birdsall and A. B. Langdon, *Plasma Physics via Computer Simulation* (Adam Hilger, Bristol, 1991).
[33] J. P. Boeuf and C. Punset, in *Dusty Plasmas*, edited by A. Bouchoule (John Wiley & Sons, 1999).
[34] J. D. Lawson, *The Physics of Charged-Particle Beams* (Clarendon Press, Oxford, 1988).
[35] M. Salimullah, P. K. Shukla, and G. E. Morfill, J. Plasma Phys. **69**, 363 (2003).
[36] S. V. Vladimirov and E. N. Tsoy, Phys. Rev. E **64**, 035402(R) (2001).
[37] M. P. Hertzberg, S. V. Vladimirov, and N. F. Cramer, Phys. Rev. E **68**, 026402 (2003).
[38] I. H. Hutchinson, Plasma Phys. Controlled Fusion **47**, 71 (2005).